Dynamics of a cellular flame after a head-on interaction with a shock wave

Hongxia Yang[a,b], Matei I. Radulescu[b]
[a] Fire & Explosion Protection Laboratory, Northeastern University, Shenyang, China
[b] Department of Mechanical Engineering, University of Ottawa, Ottawa, Ontario, Canada

1 Introduction

Shock flame interactions are common in many combustion applications ranging from the problem of deflagration to detonation transition (DDT) to supersonic propulsion applications. Since the pioneering work of Markstein [1], this problem was recognized as of prime importance in combustion processes that require higher burning rates. Markstein [1] in his classic experiments observed the head-on collision between an initially laminar flame and a shock wave. He successfully visualized a spike of unburnt gas penetrating into the burnt region. Nonetheless, the shock quickly reflected from the end wall, and the secondary interaction led to a highly turbulent flow which complicated the observation of the shock-flame complex. Later on, Rudinger [2] in his experiments found out that after the passage of the shock, the initially spherical flame evolved to a vortex ring. Other experiments done by Scarinci *et al.* proved that the interaction could increase the burning rate by shock generated turbulence and the massive deformation of the flame surface [3]. Thomas *et al.* [4] were able to visualize the flame folding caused by the incident shock and the transition to detonation resulting from the reflected shock during shocks interacting with spherical flame bubble of stoichiometric ethylene-oxygen with 50% nitrogen. It is known in these studies that the interaction could strongly disturb the flame to increase the flame surface and subsequently enhance the burning rate. The underlying mechanism of Rychtmyer-Meshkov(RM) instability, which is known to influence the curved interface deformation by generating vorticity through the baroclinic torque mechanism. However, the fact that the interactions in the experiments quickly lead to complex turbulent flow and multiple interactions make it difficult to quantify the flame deformation and acceleration induced by single shock flame interaction, to isolate the influence of a shock on the flame and recognize the underlying mechanism. Efforts also have been made in numerical simulations focusing on vorticity generation [14], flame distortion induced by successive passage of shocks [8,9], and deflagration to detonation transition process in shock flame bubble interactions caused by the reflected shock-flame interaction [10–12]. Nevertheless, the flame evolution subsequent to a single shock-flame interaction has not been quantified and clarified.

Considering the importance of shock flame interaction in the combustion process, it is of interest to quantify the increasing rate of flame surface areas and burning velocity caused by the interaction, as well as

Correspondence to: yang.hongxia@foxmail.com

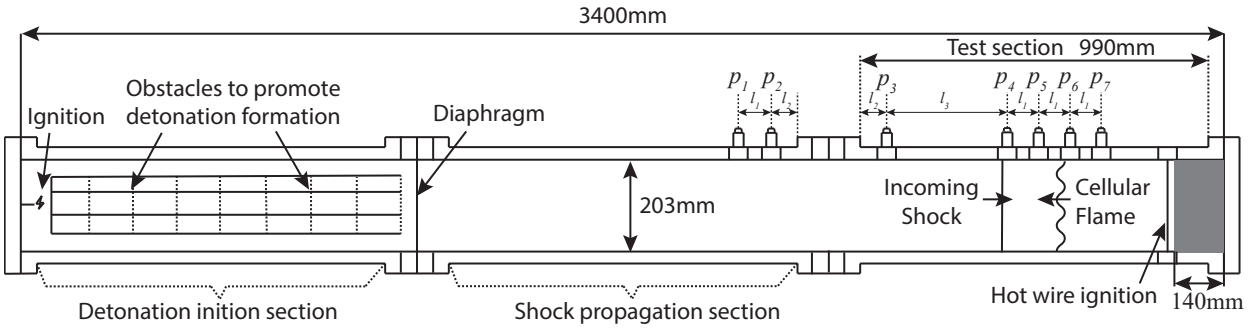

Figure 1: Schematic of the experiment setup in the shock tube, $l_1 = 102$mm, $l_2 = 51$mm, $l_3 = 406$mm.

identify the controlling mechanism. In practice, the flames would always be subject to both diffusional-thermal and hydrodynamic instabilities. In the present study, we focus on cellular flames prone to the Landau-Darrius(LD) hydrodynamic instability only. The experiments are performed at low pressure in stoichiometric hydrogen-air, such that large cells can be isolated and their deformation studied with precision after passage of a shock wave.

2 Experimental procedures

The experiments were conducted in a shock tube with dimensions of 3400mm $\times$ 19.1mm $\times$ 203.2mm, as shown in Fig 1. The channel consists of three parts: the detonation initiation section, the shock decouple section and the test section. The detonation initiation section was separated from the other two parts by a layer of aluminium foil. A series of high-frequency piezoelectric PCB pressure sensors (p1-p7) were mounted flush on the top wall of the shock tube to collect pressure signals and the arrival of the shock. A pair of optical quality glass window was installed at the test section in order to visualize the phenomenon. For each experiment, the shock tube was evacuated to a pressure less than 80 Pa. Then the detonation initiation section was filled with $C_2H_4 + 3O_2$ mixture as driver gas before filling the rest part with $2H_2/$air mixture. The gases were prepared in mixing tanks by the method of partial pressure and were left to mix for more than 24 hours. The flame was ignited by a 0.15-mm-thick hot tungsten wire mounted in the end of the test section. When the flame has propagated a sufficient distance to acquire a quasi-stationary cellular structure, the shock was initiated by triggering a detonation in the driver gas. This detonation transmitted a shock wave into the test gas, followed by a much weaker flame that did not participate in the experiment. The decoupled shock then traveled toward the test flame and interacted head-on.

A Z-type Schlieren system with a field of view of 317.5 mm was implemented to capture the shock-flame interaction process. The image sequence was recorded using a high-speed camera (Phantom v1210). The frame rate was 59,590 frames per second (fps) with a resolution of 512 $\times$ 320 and the exposure time was set to 0.468 μs.

3 Results

Figure 2 shows the superposition of stoichiometric $2H_2/$air flame fronts for the very early stage at a initial pressure of 20.7 kPa with a time interval of 0.25 ms. Note that the flame propagated from the right to left in

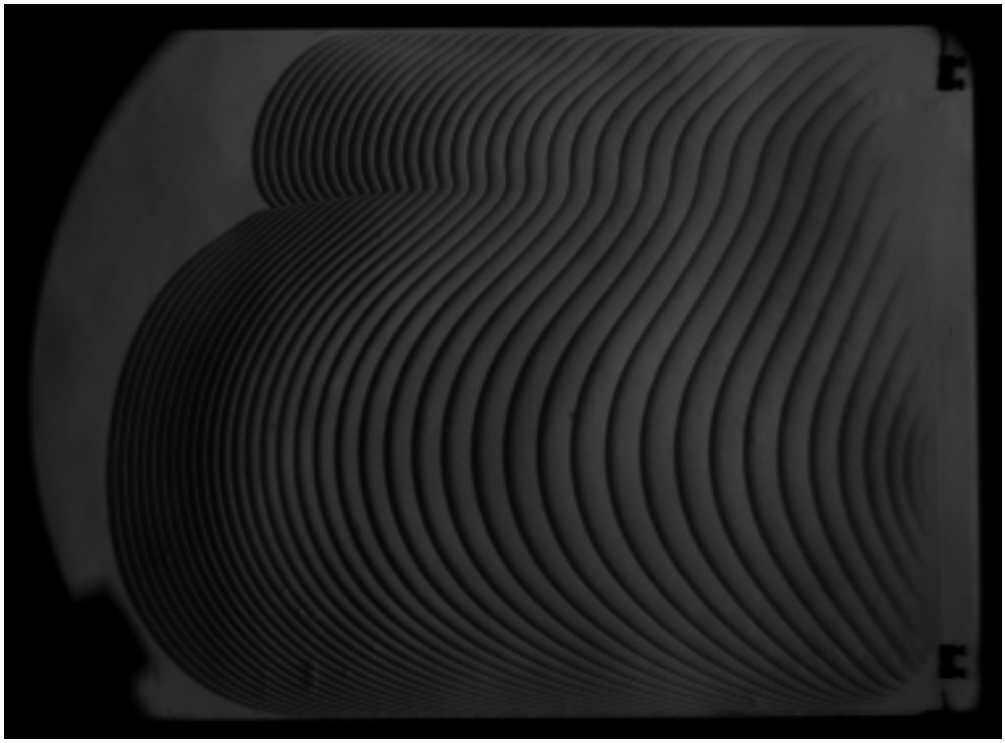

Figure 2: Superposition of flame fronts at different time for stoichiometric hydrogen air ignited by hot wire. Pressure of 20.7 kPa. Recorded at 59,590 fps. The time interval between the flame front is 0.25 ms.

the shock tube. It can be seen from the varied distance between the flame fronts in Fig.2 that, once ignited by the hot tungsten wire in the right end, the flame first slowly accelerated as the perturbation curvature increased, and then decelerated to form two cells due to the hydrodynamic instability. As the newly formed cells propagated forward, the increase of their amplitude is noticeable. Figure 3a further demonstrates the birth of new cells from the bottom large cell ensuing the formation of two cells following the later stage in Fig. 2, with an initial pressure of 17.2 kPa. The flame evolution for the pressure of 17.2 kPa shows the same trend of deceleration when the new cells emerged, as shown in Fig. 3b.

Figure 4 shows the detailed evolution of the interaction of a M_s = 1.9 shock with the stoichiometric $2H_2/$air flame at the initial pressure of 17.2 kpa. The dashed lines show the position of the pressure sensors. The first two frames show that the amplitude of the flame cusps increased as the flame moved forward. The right propagating shock can be seen in the third frame to reach the flame interface. Before the interaction, the average cell size is about 75mm. In the 3rd frame, the incident shock wave (ISW) passed half the flame front, giving rise to a curved transmitted shock wave (TSW) and a reflected expansion wave. Following the passage of the shock, the flame was flattened and pushed backwards to the burnt gas. The 4th to 7th frames show that the flame cusps reversed and the amplitude of flame cells grew due to the Richtmyer-Meshkov instability. From the last three frames, it can be observed that the flame front thickened toward the unburnt gas, characterized by forming a considerable irregular rough flame surface, as marked in the dashed line. These two figures were then analyzed in order to reconstruct the flow field and finally get the flame deformation and acceleration mechanism subsequent to the single shock-flame interaction.

The pressure profiles recorded from the pressure sensor are plotted in Fig.5a to help to understand the

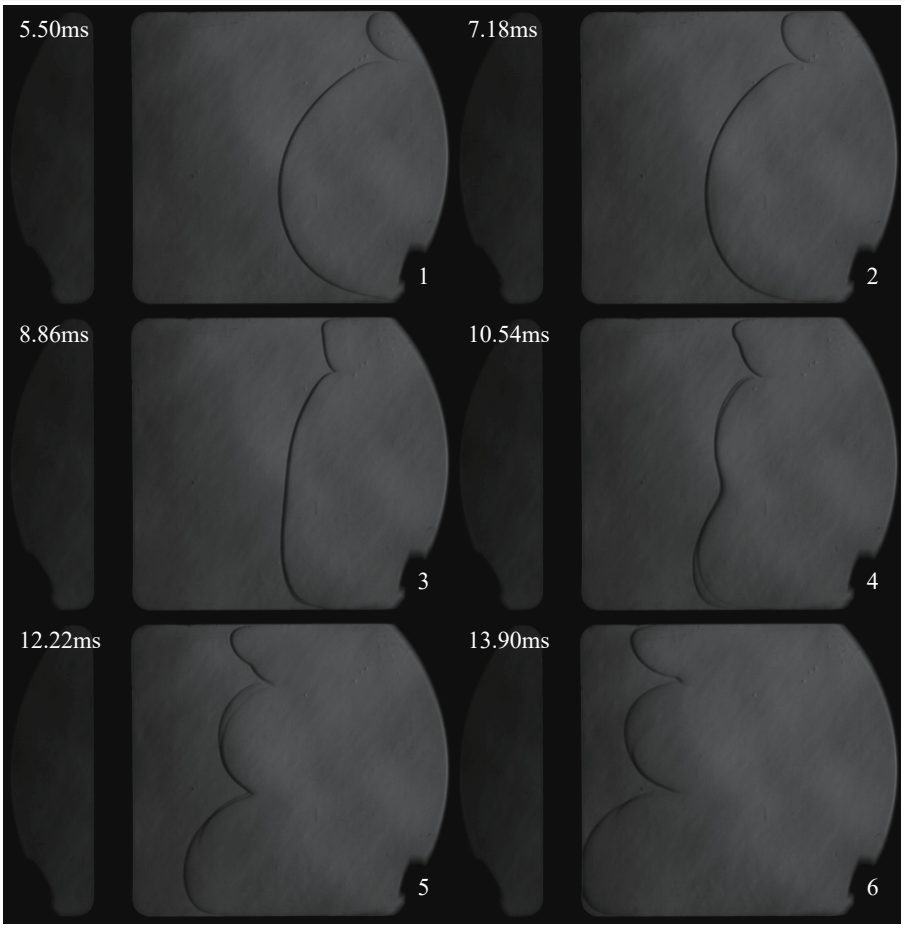

(a)

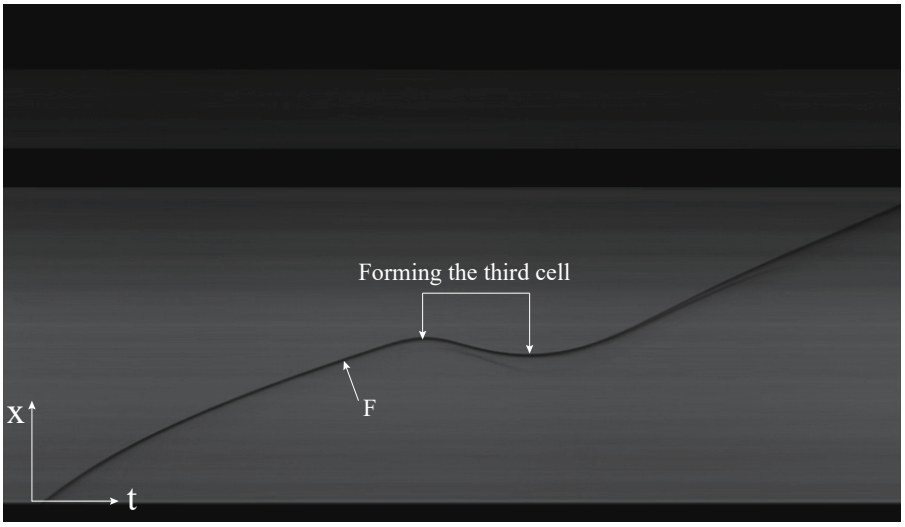

(b)

Figure 3: (a) Schlieren image sequence, (b) Space-time diagram obtain from the middle of the channel for stoichiometric hydrogen-air flame propagation from right to left. Pressure of 17.2kpa. Recorded at 59,590 fps. The time interval between the flame front in (a) is 0.25 ms.

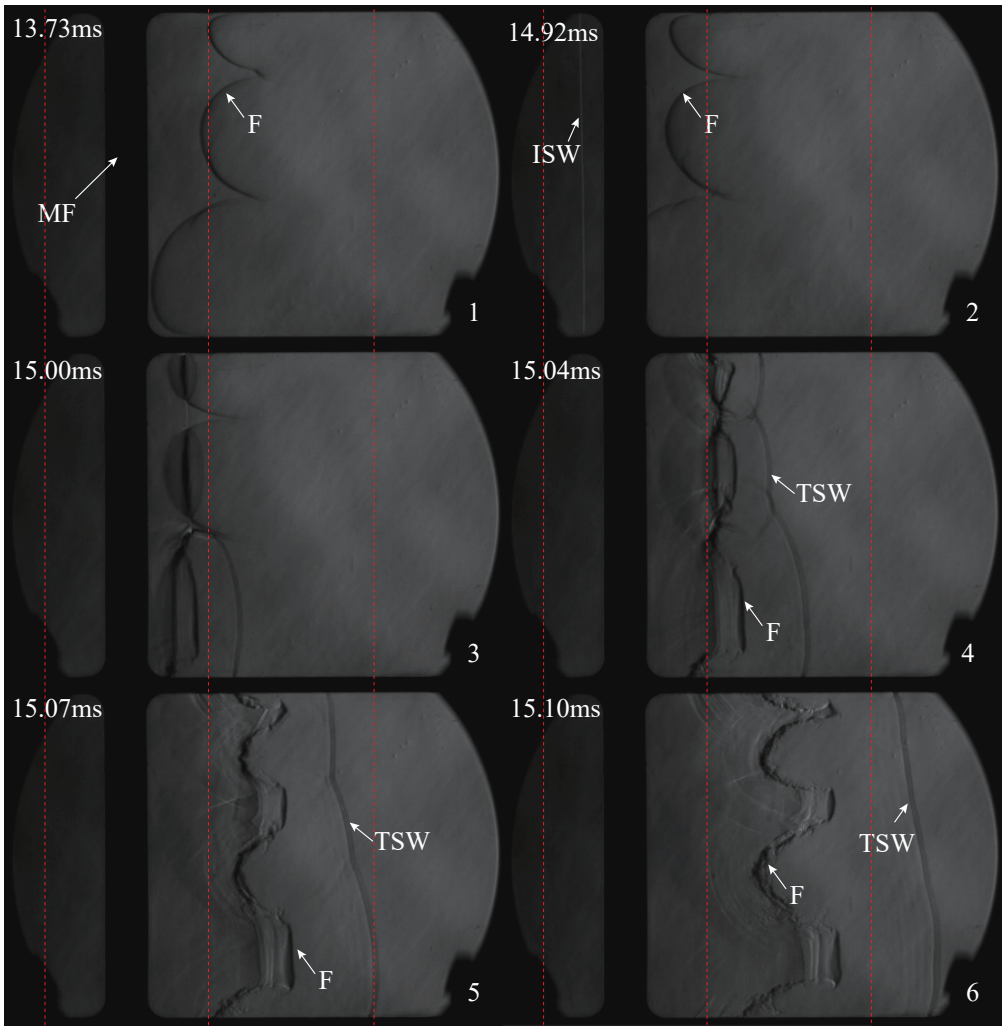

Figure 4: Schlieren image sequence of the interaction of a M=1.9 incident shock wave(ISW) with stoichiometric hydrogen-air flame(F). TSW is the transmitted shock wave, MF is the middle flange of the shock tube. Flame initial pressure of 17.2kpa. Recorded at 59,590 fps. The time interval between the flame front is 0.25 ms.

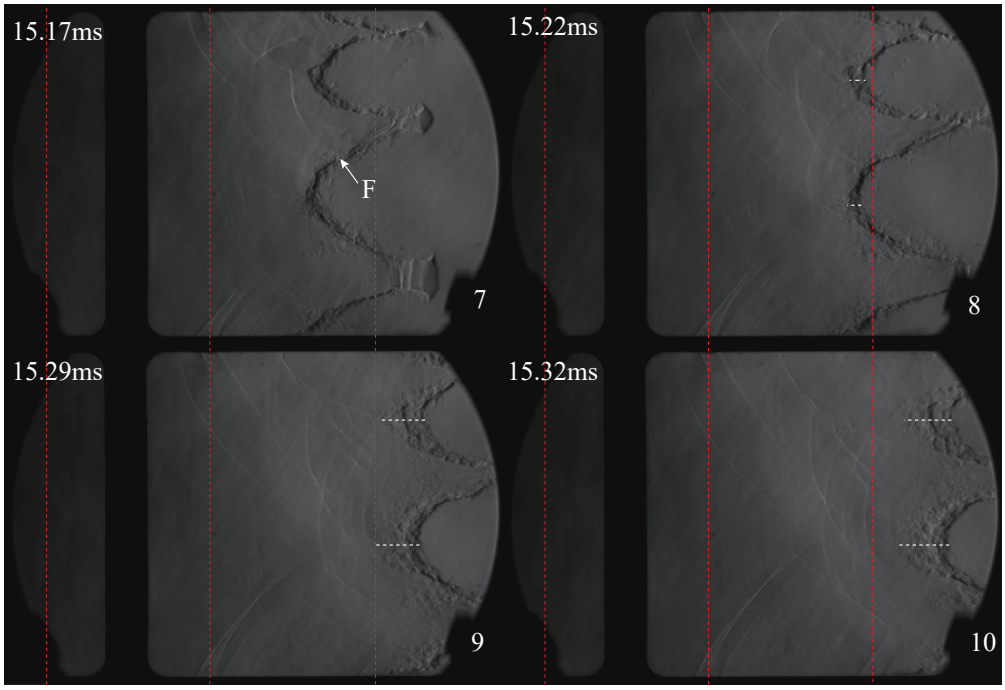

Figure 4: (continued) Schlieren image sequence of the interaction of a M=1.9 incident shock wave(ISW) with stoichiometric hydrogen-air flame(F). TSW is the transmitted shock wave, MF is the middle flange of the shock tube. Flame initial pressure of 17.2kpa. Recorded at 59,590 fps. The time interval between the flame front is 0.25 ms.

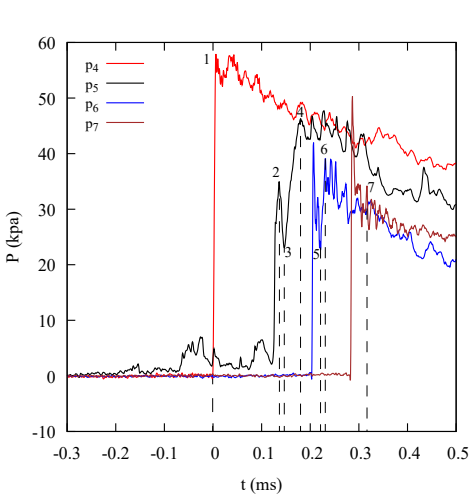

(a) Initial and overpressure signals assiciated to the interaction recorded along the channel, time 0 corresponds to the time the shock reached the 4th pressure sensor.

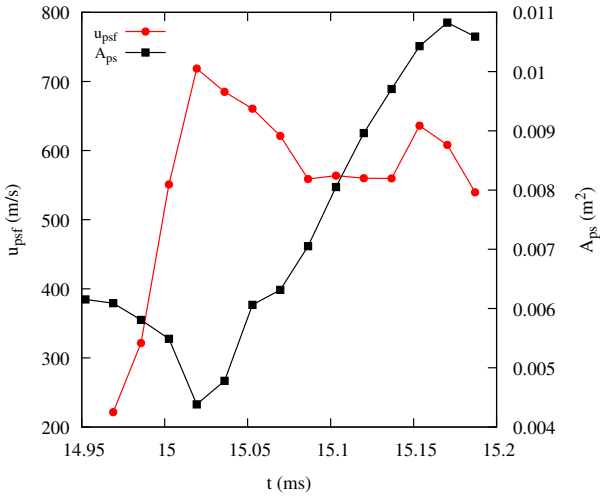

(b) Average flame propagation velocity and area evolution subsequent to the interaction, time 14.95ms corresponds to the time the flame is ignited to the shock reached the flame.

Figure 5: The pressure, flame propagation velocity and area evolution subsequent to the interaction of Fig.4.

interaction process. The decaying shock pressure profile before the interaction was recorded by P4 marked as 1, the fitted value was used to calculate the incident shock Mach number. P5 shows the flame pressure before the interaction, the pressure increase is possibly caused by the initial flame acceleration before the flame formed the cellular structure. Then marker 2 to 3 recorded the transmitted wave and the decay behind the wave, signal 3 recorded the flame arrival(4th frame in Fig.4) and the pressure increase after 3 denoted the expansion wave. The pressure decay after the passage of the transmitted shock is also recorded in P6, the pressure rise from 5 to 6 signified the arrival of the flame tip, in accordance with the 6th to 7th frame in Fig.4. The signal from 6 to 7 in P6 shows the pressure decay from the flame tip to the flame root (see frame 7th to 8 in Fig.4), signifying the pressure gradient behind the flame. Also, it can be seen that the transmitted shock strength increased when propagating toward the right end. The increase in pressure is probably from the wave sent by the accelerated flame.

Since the shock flame interaction is known as a source of disturbance to increase the flame surface and enhance the burning rate, the flame front area and propagation speed evolution subsequent to the interaction were measured to quantify the increment, as shown in Fig.5b. The flame front area was taken from the arc length of the flame interface times the channel width, assuming the interaction is quasi-two-dimensional. The average flame propagation speed was calculated from the mean distance the flame front traveled per unit time in the horizontal direction. During the passage of the shock, the left moving flame was pushed back and acquired a maximum speed of 718 m/s as the flame area decreased. When the shock has passed, the flame area linearly grew to approximately twice its original value, whereas there is a fluctuation in the flame speed. The average flame propagation speed for the flame evolution after the shock has passed is approximately 610 m/s.

Fig.6 shows the flame evolution following Fig.4 when the shock reflected back from the right end further disturbed the flame. In the first three frames, the shock traversed the flame and formed an indistinguishable

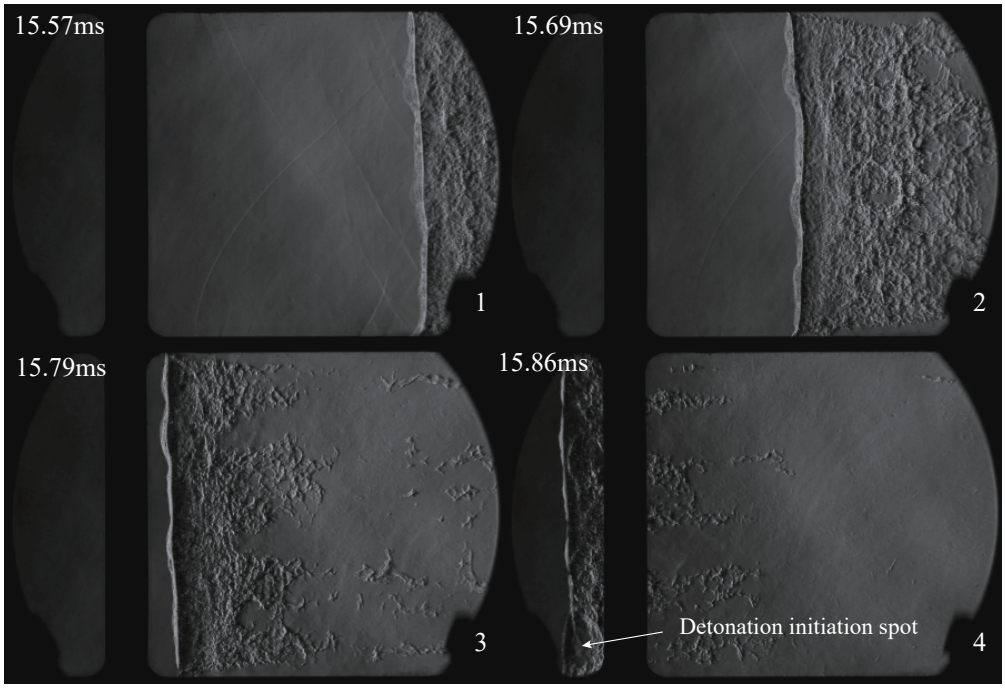

Figure 6: Schlieren image sequence of the flame coupled with the reflected as they propagated from the right to left following Fig.4.

shock-flame complex, similar to that observed by Thomas *et al.* [4] in which they define this coupling of shock and flame front as 'strange wave'. Note that the flame front was widely enlarged and developed into very fine structures. A detonation ignition spot then emerged from the bottom of the channel in the fourth frame, after which the entire front transitted to a detonation wave.

4 Discussion

The experimental sequence and pressure measurements permitted to reconstruct the flow field in order to evaluate the state of the gas head of the flame after the interaction, and evaluate the turbulent burning rate of the flame. A sketch of the reconstructed one-dimensional gas dynamic model is shown in Fig.7b. The shock-flame interaction is assumed to give rise to a transmitted shock and reflected expansion wave. We also expect a weak contact surface to establish along the material interface following the fluid element where the first shock and incident flame first occurred. The initial state across the flame was computed from the adiabatic flame model using Cantera and the thermochemical database of Li et al. [13]. The curved flame burning velocity was corrected from the free flame speed from CANTERA by considering the ratio of the flame area and channel cross-sectional area, whereas the pressure increase in state 2 was evaluated by the method of characteristics. The flame propagation velocity was measured from the mean average moving distance per unit time after the flame formed 3 cells. State 2 is then calculated by applying the mass and momentum conservation balance. The flow from state 2 to state 3 and state 1 to state 6 across the shock obey the usual shock jump equation. The expansion from state 4 to state 3 is assumed to be isentropic. For all states, a two-gamma approximation was used, where the non-reacted and reacted gas are assumed to be

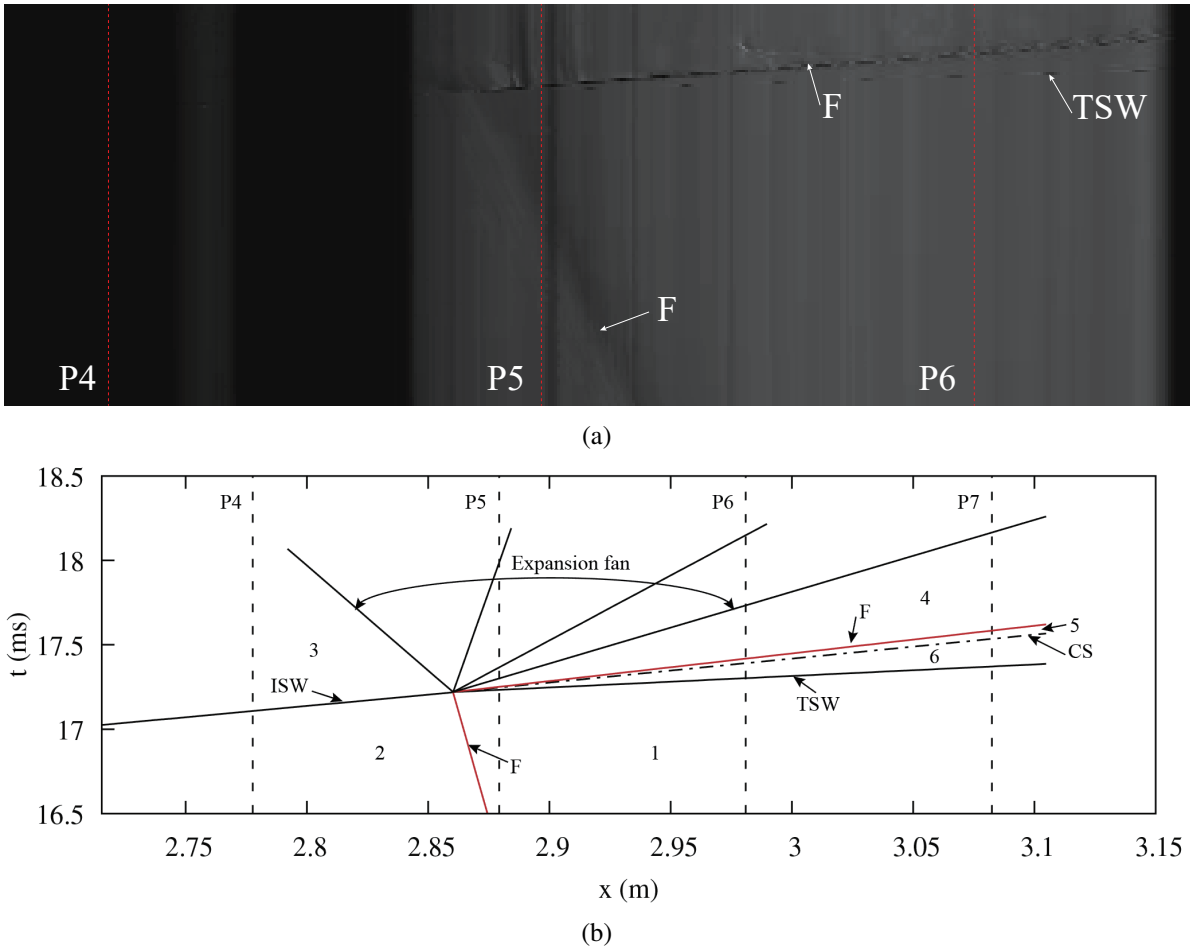

Figure 7: The space-time diagram evolution of interaction of Fig.4 (a) along the top of the channel, (b) reconstructed from the one-dimensional gas dynamic model.

polytropic gases with constant thermodynamics properties [6]. Also, the pressure is assumed to be constant for each state. A system of equations is then built from state 3 to state 6, in which the flame propagation velocity and pressure across the flame were calculated according to different guess of burning velocity. The various burning velocity was given such that the experimentally measured flame propagation speed in the laboratory frame was recovered. When this average flame propagation speed was matched, (see Fig.8), the burning velocity is approximately 21 m/s, and the pressure in state 4 is about 43 kPa. The pressure was in a good agreement with that value measured from the 5th pressure sensor marked as 2 in Fig.5a. As shown in Fig. 7, the reconstructed flow field also presents excellent agreement with the space-time diagram obtained from the top of the channel.

It is of interest to comment on whether the small perturbations observed on the large flame cells after the interaction may be due to smaller scale LD instability due to the higher flame speeds and thinner flames after the interaction. To quantify the flame enhancement due to the interaction, the free flame speed and thickness in state 2 and state 4 were computed in CANTERA. A flame thickness of 1.3 mm was obtained for the state 4, which is approximately 2.4 times smaller than the original laminar flame thickness in state 1. For the

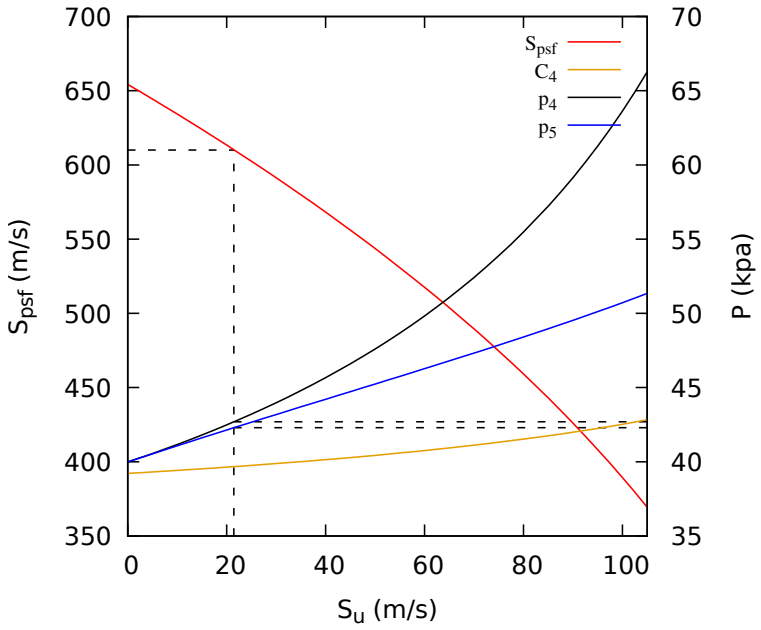

Figure 8: Reconstructed flame propagation speed, the sound speed in state 4 (C_4), the pressure in state 4 (p_4) and state 5 (p_5) in accordance with different burning velocity

burning velocity, the calculated post-shock one-dimensional burning velocity is approximately 1.7 times the one-dimensional burning velocity before the interaction and 6 times smaller than the one reconstructed from the gas dynamic model (attributed to flame wrinkling). Since the cell size of a flame scales with the thickness of the flame [7], the expected cell size after the interaction should be approximately 2-3 times smaller than the large cells. Since perturbations smaller by an order of magnitude are generally observed (see Fig. 3), the LD instability may not be the main destabilization mechanism.

Another possibility for the small scale wrinkling is through the RM instability of the flame tails, since the gases near the flame tails finds its way to form the crests of the new cells after the large scale deformation by the RM instability. It thus instructive to compare the relative growth rates of RM instability and hydrodynamic instabilities discussed above at these small scales. As shown in Fig. 8, the pressure in state 4 and state 5 across the flame is nearly constant. Thus, the cell perturbation growth rate σ for the hydrodynamic instability in nearly isobaric flow as mentioned in [5] as a function of wavenumber $k = \frac{2\pi}{\lambda}$ was calculated based on the experimental condition.

$$\sigma = kS_u \frac{\theta}{1+\theta}((1+\theta-\frac{1}{\theta})^{\frac{1}{2}} - 1) \tag{1}$$

where $\theta = {}^{T_b}/_{T_u} \approx {}^{\rho_u}/_{\rho_b}$ is the thermal expansion the gas undergoes in the flame, the subscript 'b' refers to the burnt gas and 'u' the unburnt gas. The linear perturbation growth rate subject to RM instability was also calculated from

$$\sigma_{RM} = A_t\,[u]\,k \tag{2}$$

where $A_t = \frac{\rho_u - \rho_b}{\rho_u + \rho_u}$ is the Atwood number for the unburnt and burnt densities, $[u]$ is the change in velocity of the interface caused by the passage of the shock, k is perturbed wave number. For cells with the same wave number, the growth rate ratio of cellular structure evolution caused by thermal expansion and the RM instability was obtained of approximately 0.06, suggesting that the RM instability grows much faster. We can hence attribute the small scale perturbations and the emergence of the fine structures in the last three frames in Fig.4 to RM instability, possibly coupled to exothermicity.

The preceding two mechanisms discussed neglect the boundary layers present in our thin channel experiments. It is also possible that the flame advection backwards after the shock interaction leaves a thin layer of reacted gas close to the walls. This gas would be subjected to shear and promote ignition spots for further flame development. Clearly, future study and possible numerical reconstruction should address these ambiguities.

5 Conclusion

In this study, single shock wave colliding with a cellular flame in a shock tube was studied and analyzed. Following the passage of the incident shock, the flame cusps were flattened and reversed backwards to the burnt gas subject to the Richtmyer-Meshkov instability. The one-dimensional model reconstructed the flow field and predicted the burning velocity 6 times larger than that of the post shock flame and 16 times the initial flame before the interaction. Whereas at later times, the flame front thickening showed that small cells emerged from the large reversed flame and propagated towards the unburnt gas. It is clear that the Richtmyer-Meshkov instability initially controls the reversal and elongation of the flame interface, and might have an influence on the later rough flame front. Whereas the effects of boundary layer and transverse wave on the later roughness can not be excluded. Further study will focus on the underlying mechanism for the development of detonation from the reflected shock-flame complex.

Acknowledgement

The authors thank NSERC for the financial support. H.Y. thanks China Scholarship Council (CSC) and NSFC grant (51774068) for the financial support.

References

[1] Markstein, G. H. (1957, January). A shock-tube study of flame front-pressure wave interaction. In Symposium (International) on Combustion (Vol. 6, No. 1, pp. 387-398). Elsevier.

[2] Rudinger, G. (1958). Shock wave and flame interactions. Combustion and Propulsion, 153-182.

[3] Scarinci, T., Lee, J. H., Thomas, G. O., Bambrey, R., Edwards, D. H. (1993). Amplification of a pressure wave by its passage through a flame front. Progress in Astronautics and Aeronautics, 152, 3-3.

[4] Thomas, G., Bambrey, R., Brown, C. (2001). Experimental observations of flame acceleration and transition to detonation following shock-flame interaction. Combustion Theory and Modelling, 5(4), 573-594.

[5] Liberman, M. A., Bychkov, V. V., Golberg, S. M., Book, D. L. (1994). Stability of a planar flame front in the slow-combustion regime. Physical Review E, 49(1), 445.

[6] R. S. Chue, J. F. Clarke, and J. H. Lee, Chapman-jouguet deflagrations, Proceedings of the Royal Society of London Series a-Mathematical Physical and Engineering Sciences, vol. 441, no. 1913, pp. 607623, 1993.

[7] Law, C. K., Sung, C. J. (2000). Structure, aerodynamics, and geometry of premixed flamelets. Progress in energy and combustion science, 26(4-6), 459-505.

[8] Ju, Y., Shimano, A., Inoue, O. (1998, January). Vorticity generation and flame distortion induced by shock flame interaction. In Symposium (International) on Combustion (Vol. 27, No. 1, pp. 735-741). Elsevier.

[9] Jiang, H., Dong, G., Chen, X., Li, B. (2016). A parameterization of the RichtmyerMeshkov instability on a premixed flame interface induced by the successive passages of shock waves. Combustion and Flame, 169, 229-241.

[10] Oran, E. S., Gamezo, V. N. (2007). Origins of the deflagration-to-detonation transition in gas-phase combustion. Combustion and Flame, 148(1-2), 4-47.

[11] Dong, G., Fan, B., Ye, J. (2008). Numerical investigation of ethylene flame bubble instability induced by shock waves. Shock Waves, 17(6), 409-419.

[12] Zhu, Y., Dong, G., Liu, Y. (2013). Three-dimensional numerical simulations of spherical flame evolutions in shock and reshock accelerated flows. Combustion Science and Technology, 185(10), 1415-1440.

[13] Li, J., Zhao, Z., Kazakov, A., Dryer, F. L. (2004). An updated comprehensive kinetic model of hydrogen combustion. International journal of chemical kinetics, 36(10), 566-575.

[14] Picone, J. M., Boris, J. P. (1988). Vorticity generation by shock propagation through bubbles in a gas. Journal of Fluid Mechanics, 189, 23-51.